mater.scichina.com link.springer.com Published online 2 August 2022 | https://doi.org/10.1007/s40843-022-2191-9

Manufacture of porous metallic glass using dissolvable templates

Jianan Fu[1], Zhen Li[2], Zehang Liu[1], Xin Li[1], Wenxin Wen[1], Fei Sun[1], Luyao Li[1], Jinbiao Huang[1], Wenqing Ruan[1], Shuai Ren[1], Zhenxuan Zhang[1], Xiong Liang[1] and Jiang Ma[1*]

ABSTRACT A facile, precise, and controllable manufacturing technology is desired for hierarchical functional surfaces. In this work, we successfully manufactured porous metallic glass using a water-dissolution material as template and the excellent thermoplastic property of metallic glass. The prepared micro/nanostructures have excellent tunability, and the proposed approach can be used to prepare large-area disordered porous structures and ordered regular arrays with nanoscale replication accuracy. In particular, the disordered porous structure prepared by the dissolvable template strategy exhibits a water contact angle of ~140° and an oil contact angle of ~0°, making it suitable for oil/water separation. It also shows stable wettability after being soaked in strong acid or alkali environments and maintains a ~130° water contact angle and a ~4° oil contact angle even after severe wear. The proposed strategy also possesses excellent recycling properties. We reconstructed porous structures on the same surface three times and found no significant change in wettability for each reconstructed porous structure. Our research provides a facile and controllable approach for the preparation of hierarchical porous structures and paves the way for the design of other functional surfaces.

Keywords: dissolvable templates, metallic glass, porous structure, wettability, recycling properties

INTRODUCTION

Improving the utilization rate of material space contributes to the development of new materials with unique properties. Porous materials have recently attracted attention due to their characteristics, such as large specific surface area, high specific strength, and abundant active sites. Porous materials such as zeolites [1,2], porous organic polymers [3,4], and metal-organic frameworks [5,6] have been reported and are widely used in sensors [7,8], electromagnetic shielding [9,10], catalysis [11–13], and other fields. Various methods, mainly including soft or hard templating methods and template-free methods, have been developed to form porous materials. The pore size of porous materials prepared by template methods is easy to regulate due to the regular arrays and patterns of the template. However, the removal of the template is tedious and not environmentally friendly, thus hindering scaled-up production [14,15]. The template-free method is a simple process and has great advantages in the preparation of large-area porous materials; however, it faces the problem of high cost [16,17]. Therefore, convenient and low-cost synthesis methods must be explored for the preparation of porous materials. Metallic glasses (MGs), i.e., amorphous alloys, have been extensively studied for structural and functional applications since their discovery because of their excellent properties [18–26]. Different from conventional metallic materials, MGs can be processed similarly to plastic when heated to a certain temperature range due to their unique disordered atomic structure. Owing to this feature, the advanced processing technology of MG thermoplastic forming (TPF) has been explored. To date, many micro/nanostructures have been achieved through TPF, such as nanowires [27,28], precision gratings [29,30], and precision microfluid [31]. However, the formation of hierarchical porous MGs is rarely reported due to the lack of templates and the difficulty of the preparation by other processes. The existing preparation methods for porous structure on MGs [32,33] mainly include dealloying [34,35], one-pot pulse anodization [36], pitting [37], foaming [38,39], infiltration [40,41], and space holders [42,43]. However, dealloying, one-pot pulse anodization, pitting, and some infiltration methods cannot guarantee the original amorphous properties of MGs; as a result, the unique properties of MGs cannot be maximized. Foaming methods have several disadvantages, such as a long preparation period and difficulty in regulation. Some other methods are also plagued by technical and preparation safety problems.

In this study, we propose a low-cost, controllable, environmentally friendly, and dissolvable precision template strategy to prepare porous structures on the MG surface using salt as a template *via* TPF. The template only takes ~5 min to completely dissolve in water. A transition from irregular porous to regular morphology can be achieved by artificially designing the salt template shape, and the surface pore size can be regulated by changing the size of the salt particles. The irregular porous MG obtained by the dissolvable template strategy shows a water contact angle (WCA) of ~140° and an oil contact angle (OCA) close to 0°. When porous MG is exposed to a strong acid or alkali environment, its WCA and OCA do not change significantly and remain at 130° and 4°, respectively, even after severe wear. In addition, the porous MG still keeps its original amorphous structure, which allows the repeated formation of

[1] Shenzhen Key Laboratory of High Performance Nontraditional Manufacturing, College of Mechatronics and Control Engineering, Shenzhen University, Shenzhen 518060, China
[2] Department of Mechanics and Aerospace Engineering, Southern University of Science and Technology, Shenzhen 518055, China
* Corresponding author (email: majiang@szu.edu.cn)

the porous structure and the recovery of the damaged porous structure. Our study offers a new strategy for the high-throughput preparation of porous structure on MG surface and extends the application of MG functional surface in various fields.

EXPERIMENTAL SECTION

Raw materials

$Pt_{57.5}Cu_{14.7}Ni_{5.3}P_{22.5}$ (Pt-based MG) was selected as a model material due to its excellent thermal stability and TPF ability (Fig. S1) [27]. $Pt_{57.5}Cu_{14.7}Ni_{5.3}P_{22.5}$ alloy ingots with nominal composition were prepared by melting Pt, Cu, Ni, and P (>99.9% purity). The alloy ingots were then transformed into Pt-based MG bars with a diameter of 5 mm by copper-mold suction casting. The prepared Pt-based MG bars were cut into 1–2 mm thick Pt-MG plates and polished on both sides for use to facilitate TPF.

Preparation of NaCl templates

The original NaCl solids were purchased from Sinopharm Chemical Reagent Co., Ltd. The purchased NaCl particles were placed in a grinding bowl for grinding, and NaCl was screened out after grinding. Internal ~150 and ~110 μm sieves were used to screen ~150 and ~110 μm NaCl powders, respectively, which were then dried and used as templates during TPF.

The ~3 μm NaCl template was prepared through recrystallization. A sufficient amount of original NaCl solids were dissolved in distilled water to form a saturated solution, which was slowly dropped into 1000 mL of analytical reagent ethanol under vigorous stirring (1500 r min^{-1}). The NaCl particles slowly recrystallized and precipitated. The precipitate was then collected by filtration, washed with ethanol (10 mL × 2), and then dried under reduced pressure to prepare NaCl particles with a size of ~3 μm.

The arrays with uniform circles, squares, and triangles were fabricated using a picosecond laser on polished NaCl crystal sheets.

Dissolvable template strategy

The porous structure was prepared from salt particles as a template. The polished Pt-MG plate and the NaCl particles were stacked in a designed mold with a through-hole of 5.5 mm in the center. The mold was then placed in a vacuum heating chamber. When the chamber was in a high vacuum environment (3×10^{-3} Pa), the entire chamber was heated at a rate of 30 K min^{-1}. After the temperature rose to ~540 K, the MG in the mold was applied with a pressure of 210 MPa for 10 s at a loading rate of 0.05 mm s^{-1} using the indenter (Fig. S2). The sample was taken out of the chamber and then placed in distilled water to remove the salt template on the porous MG.

MGs with regular arrays on the surface were also formed by hot pressing at the temperature of ~540 K and the pressure of 30 MPa with a loading rate of 0.05 mm s^{-1}. When the temperature was cooled down to room temperature, the samples were placed in distilled water for dissolution. The specific experimental parameters for the preparation of MG with regular arrays are listed in Table S1.

Multiscale structural characterization

X-ray diffraction (XRD; Rigaku MiniFlex 600) with Cu-Kα radiation was used to ascertain the amorphous properties of the original Pt-based MG and porous MG. Differential scanning calorimetry (DSC; Perkin-Elmer DSC-8000) at a heating rate of 20 K min^{-1} was used to detect the glass transition temperature (T_g) and crystallization temperature (T_x) of the original Pt-based MG and supercooled liquid region (SLR). An FEI Quanta 450 FEG scanning electron microscopy (SEM) instrument was used to characterize the surface morphologies of the porous MG. JEM-2100F transmission electron microscopy (TEM) with energy dispersive spectroscopy (EDS) was applied to examine the atomic structure and elemental distributions of porous MG. A computer tomography system (CT; YXLON FF35 and Sanying precision instruments-nano Voxel3000d, China) was used to scan the three-dimensional (3D) topography of the porous structure and analyze the pore volume. A laser scanning confocal microscope (VK-X250K, Keyence, Japan) was employed to visualize the microstructure parts. A droplet shape analyzer (DSA100S, Krüss, Germany) with a 1 μL volume of water droplets was used to measure the CA of the microstructure surface. An electronic balance (Sartorius Quintix35-1CN, measurement accuracy 0.01 mg) was applied to measure the weight of the samples.

RESULTS AND DISCUSSION

Characterization of the porous MG

Fig. 1a schematically shows the quick preparation of porous MGs. The salt template is stacked to the MG. Pressure is applied when the temperature is in the SLR of the Pt-based MG, followed by its placement in water for dissolution. The dissolution of the porous MG in water is displayed in Fig. 1b (Movie S1 records the dissolution process). In this clear dissolution process, the salt template on the surface is completely dissolved in a short time within 5 min. All these findings show that the porous MG obtained by the dissolvable template strategy has the advantage of easy preparation and demolding. Fig. 1c depicts the porous MG surface micromorphology. Large and small pores cover the MG surface, resulting in a hierarchical porous structure. The 3D porous morphology is presented in Fig. 1d (Fig. S3), and the corresponding pore volume size was characterized in Fig. 1e. The volume distribution of various colors can be seen in the volume map, further demonstrating that the surface is a composite of many different pore sizes. The characteristics and atomic structures of the prepared porous structures were also examined. Fig. 1f reveals the high-resolution TEM (HRTEM) image of the porous structure. The disordered atomic structure indicates that the porous structure still has an amorphous nature, which is also confirmed by the diffraction rings in the inset. Fig. 1g displays the low-resolution TEM image and elemental mapping results of the porous structure. Elements Pt, Cu, Ni, and P are homogeneously distributed on the porous structure. The state inside the salt templates before and after TPF was observed to investigate the mechanism of forming porous structures during TPF. The gaps between the salt particles were observed prior to TPF (Fig. S4). When the MG is still in the SLR, its excellent flowability allows it to fill these gaps to form the nanowalls. Meanwhile, the individual salt particles are partially coated by the MG to form the corresponding large porous structure. The small holes in the nanowalls are formed by the close contact between salt particles, making it impossible for the MG to fill these areas. The details of the forming mechanism can

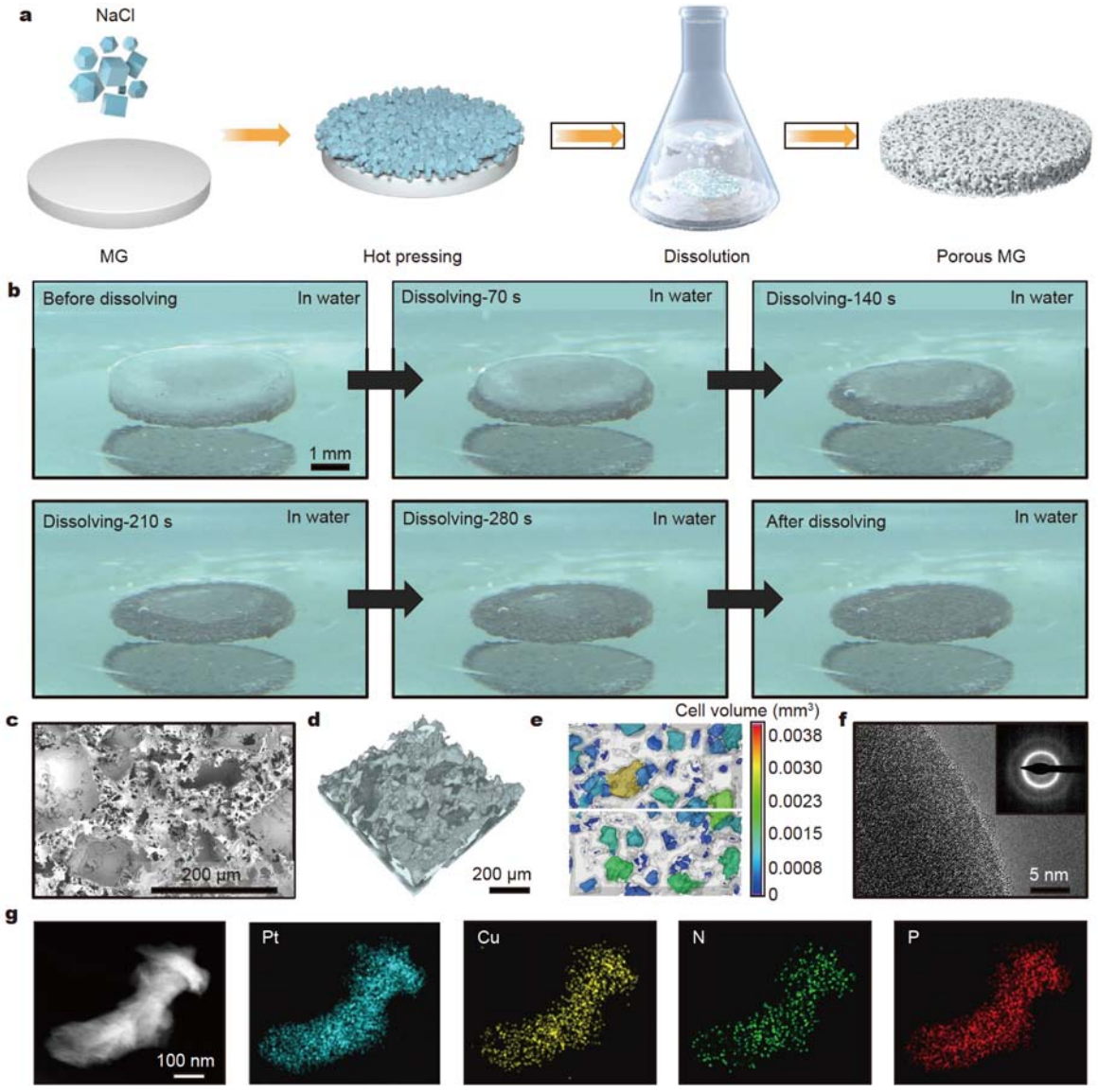

Figure 1 Characterizations of the porous MG. (a) Schematic of the porous MG fabrication; (b) dissolution of the porous MG in water; (c) SEM image of the porous MG; (d) CT image of the porous MG; (e) cell volume distribution of the porous MG; (f) HRTEM image of the porous MG (the inset is an electron diffraction image of the selected region); (g) element distribution of the porous MG by EDS.

be found in Supporting Note S1.

Dissolvable template strategy for designing porous MG morphology

A major challenge is to develop advanced materials whose structural size and shape can be artificially regulated. The dissolvable template strategy shows remarkable advantages in this regard, because it allows the simple regulation of the size and shape of the structure. Fig. 2a–c show the morphologies of the irregular porous structure obtained using three different particle sizes of salt particles, and the corresponding magnified images can be found in the insets. The size of the porous structure can be regulated using different sizes of salt particles, and the 3D morphology of the porous structures (Fig. 2d–f) further indicates the tunability of the porous structure. In addition, the size distribution of the irregular porous structure was determined by SEM images (Fig. S5), and the average pore size matches the size of the salt particles used. The application of salt as a template enables the fabrication of irregular and regular structures. Benefiting from the easy processing of the salt material, three different microstructures of square, triangle, and circle have been designed on the salt surface. Fig. 2j, n, and r show the square, triangular, and circular arrays of microstructures on the salt template surface, and the individual shape templates can be found in the insets. The neat structure is arranged on the salt template surface. When these salt templates are used for TPF, the large-area structure can be replicated on the MG surface (Fig. 2g–i). The morphology changes of the salt template surface and the MG surface after employing the dissolvable template strategy were compared to further investigate the microstructure formed on the MG surface. Fig. 2k, o, and s show the square, triangular, and circular array structures replicated on the MG using salt templates of different shape sizes, and the corresponding single shape structures are presented in the insets. The 3D structures of squares, triangles, and circles on the MG surface were observed (Fig. S6). A comparison of the size of the salt

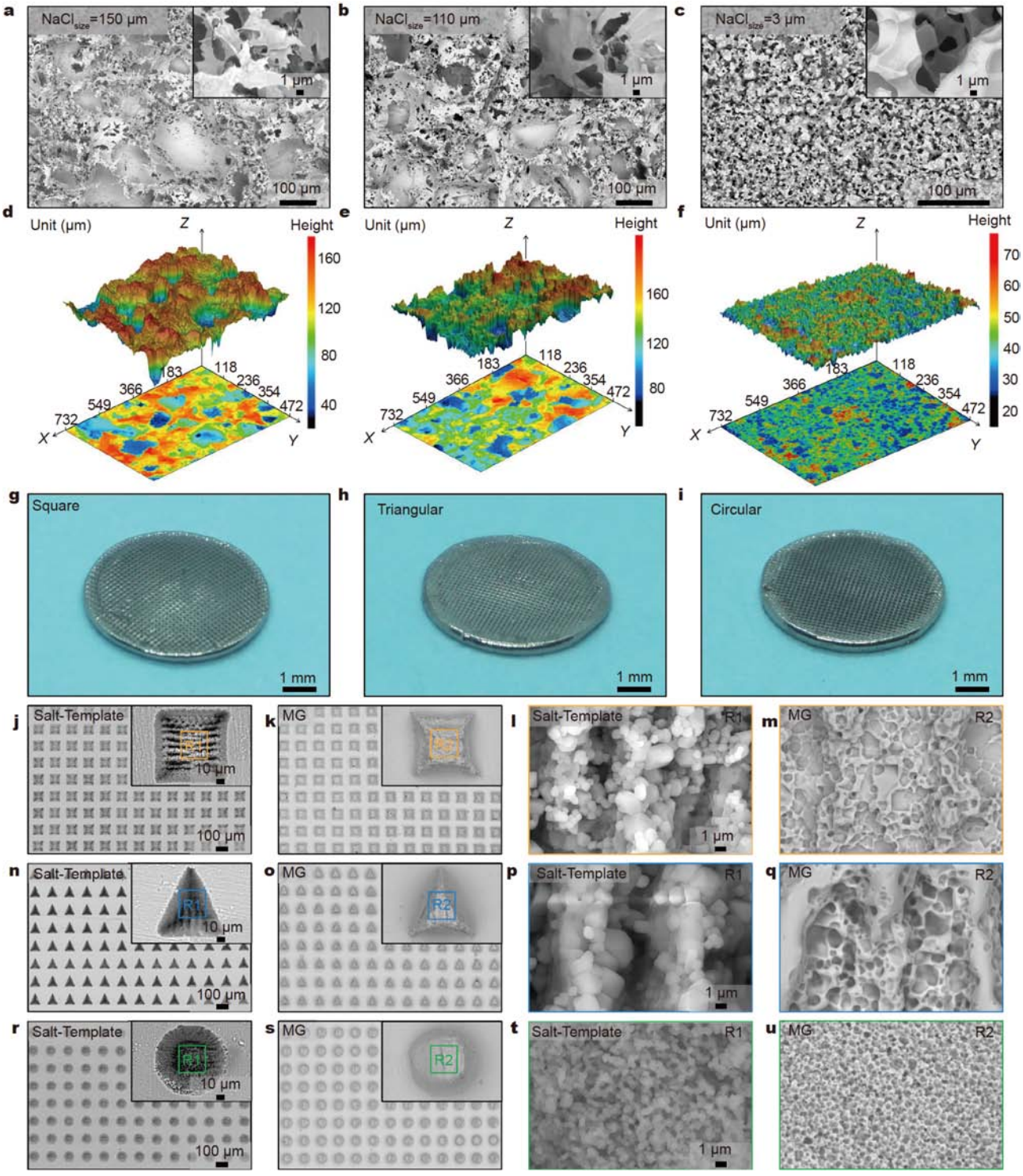

Figure 2 Dissolvable template strategy for designing porous MG morphology. (a) Porous morphology obtained using salt particles with a particle size of ~150, (b) ~110, and (c) ~3 μm (the inset is the partial magnification image); (d) 3D porous morphology obtained using salt particles with a particle size of ~150, (e) ~110, and (f) ~3 μm; images of the MG with (g) square array, (h) triangular array, and (i) circular array; (j, n, r) SEM images of the square, triangular, and circlular salt templates (the insets are the respective salt template images); (k, o, s) SEM images of the MG with square, triangular and circle arrays (the insets are the respective single pattern images); (l, p, t) bottom magnifications of the square, triangular, and circle salt templates; (m, q, u) top magnifications of the MG with square, triangular and circle arrays.

template structure and that of the microstructure replicated on the MG reveals that the maximum replication accuracy error is only 2% (Table S2). The use of salt pits as templates can successfully replicate their corresponding structures on the MG. The bottom of the salt template exhibits numerous nanoscale salt particles during processing (Fig. 2l, p, and t), and this structure is also perfectly replicated during TPF and forms an irregular porous structure (Fig. 2m, q, and u). This finding

indicates that MG can replicate micro/nanoscale precision structures.

Given that the MG flow in SLR behaves as a Newtonian fluid, Hagen-Poiseuille Equation (1) can be used to describe the MG forming behavior [27].

$$P = 32\eta Lv / d^2, \quad (1)$$

where P is the pressure, η is the viscosity, L and d are the length and diameter through a channel, respectively, and v represents the velocity.

Equation (1) is only applicable for cylindrical channels and still has limitations for channels with complex shapes. In this regard, the equivalent diameter (d_e) is introduced to make the equation suitable for various shapes of channels [27] as follows:

$$P = 32\eta l^2 / t d_e^{\,2}, \quad (2)$$

where d_e is the equivalent diameter of the channel, and t is the filling time.

According to Equation (2), combined with the parameters set during the experiment (Table S1), the calculated P_{theory} of the formed regular array structure is in good agreement with the P_{actual} in the experiment.

Some templates used in previous TPF and their properties are summarized (Table S3) [27,30,44–51]. Compared with the previous templates, NaCl templates have advantages such as low-cost, recyclability, and environmentally friendly release. Meanwhile, NaCl can be used as a template to prepare regular arrays of patterns and irregular porous structures on MG, and the replication accuracy of the prepared structures can be extended to nanoscale.

Wettability of the porous MG

The porous structure on the MG surface could lead to many excellent functional properties, one of which is wettability. Fig. 3a, b display the dynamic CA performance of the porous MG. The WCA shows excellent hydrophobic characteristics of ~140° after being stable, and the OCA shows lipophilic characteristics close to 0° (Movie S2 records the process of wettability change). Compared with the ~70° WCA and ~10° OCA of the original smooth Pt-MG plate (Fig. S7), the introduced porous structure has changed the wettability of the surface. Wenzel and Cassie models can be used to describe the changes in wettability induced by micro/nanostructures. The Wenzel model considers that the structure introduced on the surface provides a space for filling the liquid so that the wettability of the surface is enhanced [52]. The corresponding Equation (3) of this model is as follows:

$$\cos\theta^* = r\cos\theta_y, \quad (3)$$

where θ^* represents the OCA of the porous MG, r shows the roughness factor, and θ_y is the OCA of a smooth surface.

This equation explains that the original lipophilicity of the Pt-MG plate is enhanced by the porous MG surface. The Cassie model is a description of wettability transformation. It assumes that when water drops on a surface with a microstructure, the air becomes trapped in the microstructure and changes the CA [53]. Given that the surface of the porous MG is composed of micropores and nanowalls, Equation (4) provided by this model can be used to explain the WCA change of the porous structure:

$$\cos\theta^* = -1 + f_{LS}\left(\cos\theta_y + 1\right), \quad (4)$$

where θ^* is the WCA of the porous MG, f_{LS} represents the geometrical area fraction of the solid–liquid interface, and θ_y is the WCA of a smooth surface [53].

Given the excellent lipophilicity and hydrophobicity of the porous MG, oil/water separation experiments were carried out (Fig. 3c and Movie S3). After a drop of oil falls on the surface of distilled water after Sudan Red B dyeing, porous MG can absorb the oil droplets from the water surface in a short time without removing the water. This feature facilitates the extended application of the porous MG in the field of decontamination. In addition, the wettability of porous MG surfaces under severe conditions was also investigated. Fig. 3d, h exhibit the surface morphology of the porous MG after being immersed in 1 mol L^{-1} HCl and KOH for 5 days, respectively, and the mass change of the porous MG during this period is summarized in Fig. 3e, i. The porous structure of the surface is the same as that of the original porous MG after being exposed to a severe environment under SEM, and the masses tested at regular intervals are similar to the initial masses. Fig. 3f, g, and j, k present the wettability of the porous MG surface after exposure to strong acid and strong alkali, respectively. The WCA and OCA show a striking agreement with those of the original porous MG. These results indicate that the prepared porous MG is an advanced material with excellent chemical stability. Mechanical stability is a key parameter for practical functional applications [54]. Hence, the mechanical durability of porous MG surfaces was evaluated. The prepared porous MG was placed on 2000 mesh sandpaper and worn back and forth at 35 kPa 10 times (Fig. S8), after which the structure and wettability of the surface were characterized. Fig. 3l, m show the surface morphology of the porous MG before and after wear. The upper morphology of the porous structure has been worn away, and the lower porous structure is still retained. Fig. 3n, o depict the wettability of the porous MG after wear. The WCA is slightly altered after wear but still maintains the hydrophobic properties of ~130°. Meanwhile, the OCA does not change significantly. This mechanical stability allows the use of the porous MG in severe environments.

Reconstruction of the porous MG

Structural damage during service will lead to the failure of the entire workpiece; hence, the reusability of materials must be improved. The reconstruction ability of the porous MG with functional properties was evaluated. Fig. 4a shows the diagram of reconstructing porous MG. When the structural properties of the material surface are changed or damaged, the entire porous structure on the MG surface is erased, and the porous structure is prepared again by the same TPF process. The porous structure is constructed three times on the same MG through this cycle, and the XRD pattern of the material after each reconstruction is shown in Fig. 4b. The original porous MG and the reconstructed samples exhibit typical amorphous peaks. In addition, the weight loss per erasure was recorded during reconstitution and summarized in Fig. 4c. The erased weights are 0.016 and 0.019 g for the second and third cycles of the porous structure, respectively, indicating that the weight loss during erasure is smaller than the initial weight. This finding also demonstrates the high reusability of the porous material. Fig. 4d shows the surface morphology of the porous MG after the first cycle, and the magnified image is also inserted. The WCA and OCA of the porous MG after the first cycle are shown in Fig. 4e, f, respectively. The porous structure is then erased and reconstructed, and the surface

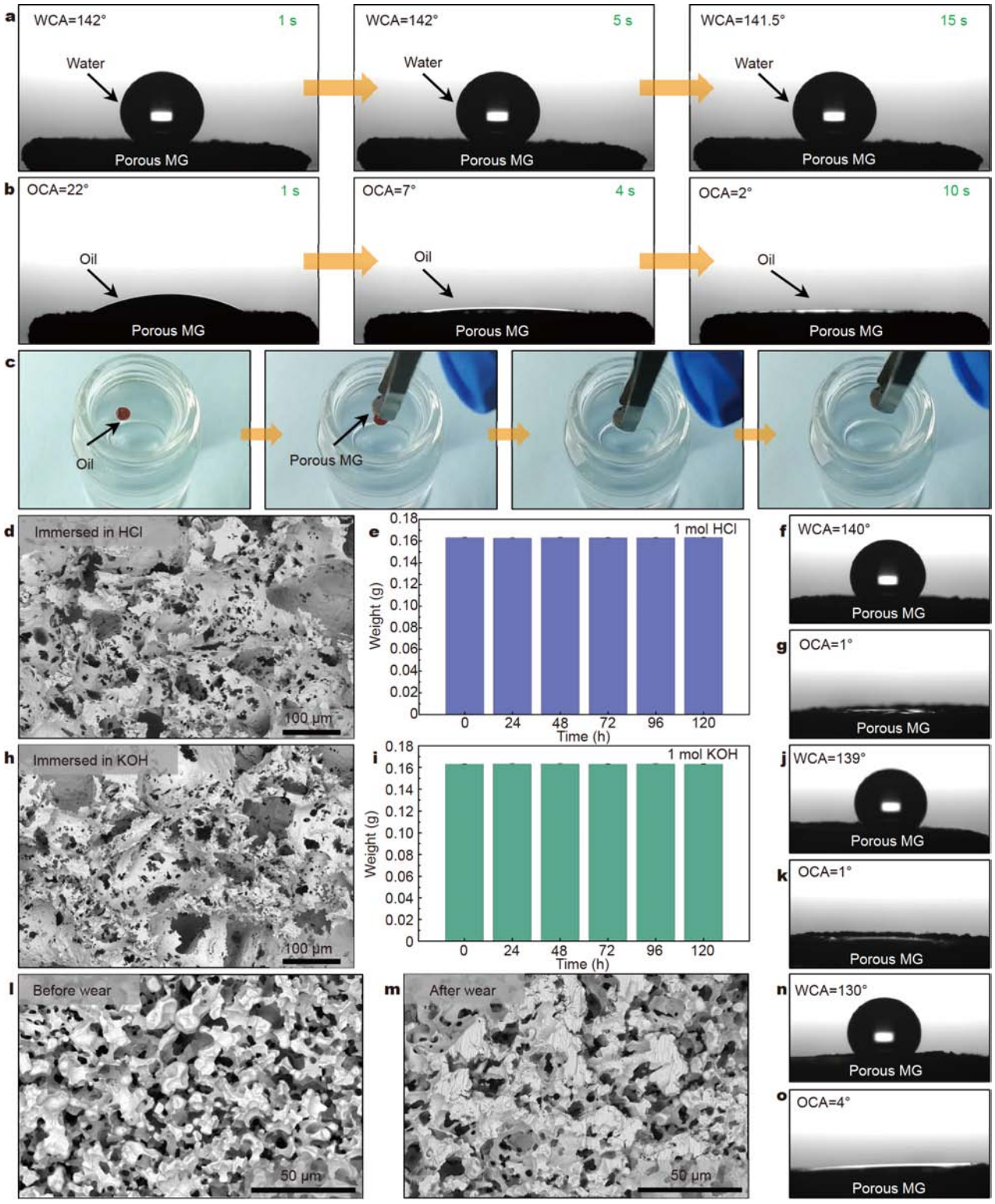

Figure 3 Wettability of the porous MG. (a) WCA of the porous MG at 1, 5, and 15 s; (b) OCA of the porous MG at 1, 4, and 10 s; (c) oil/water separation experiment; (d) morphology of the porous MG immersed in HCl (1 mol L^{-1}) after 120 h; (e) weight change of the porous MG immersed in HCl; (f) WCA of the porous MG after being immersed in HCl; (g) OCA of the porous MG after being immersed in HCl; (h) morphology of the porous MG immersing in KOH (1 mol L^{-1}) after 120 h; (i) weight change of the porous MG immersed in KOH; (j) WCA of the porous MG after being immersed in KOH; (k) OCA of the porous MG after being immersed in KOH; (l) morphology of the porous MG before wear; (m) morphology of the porous MG after wear; (n) WCA of the porous MG after wear; (o) OCA of the porous MG after wear.

morphology of the reconstructed structure is shown in Fig. 4g. The obtained surface morphology is similar to that in the first cycle, and the second constructed surface exhibits the same wettability as the first cycle (Fig. 4h, i). The porous MG is

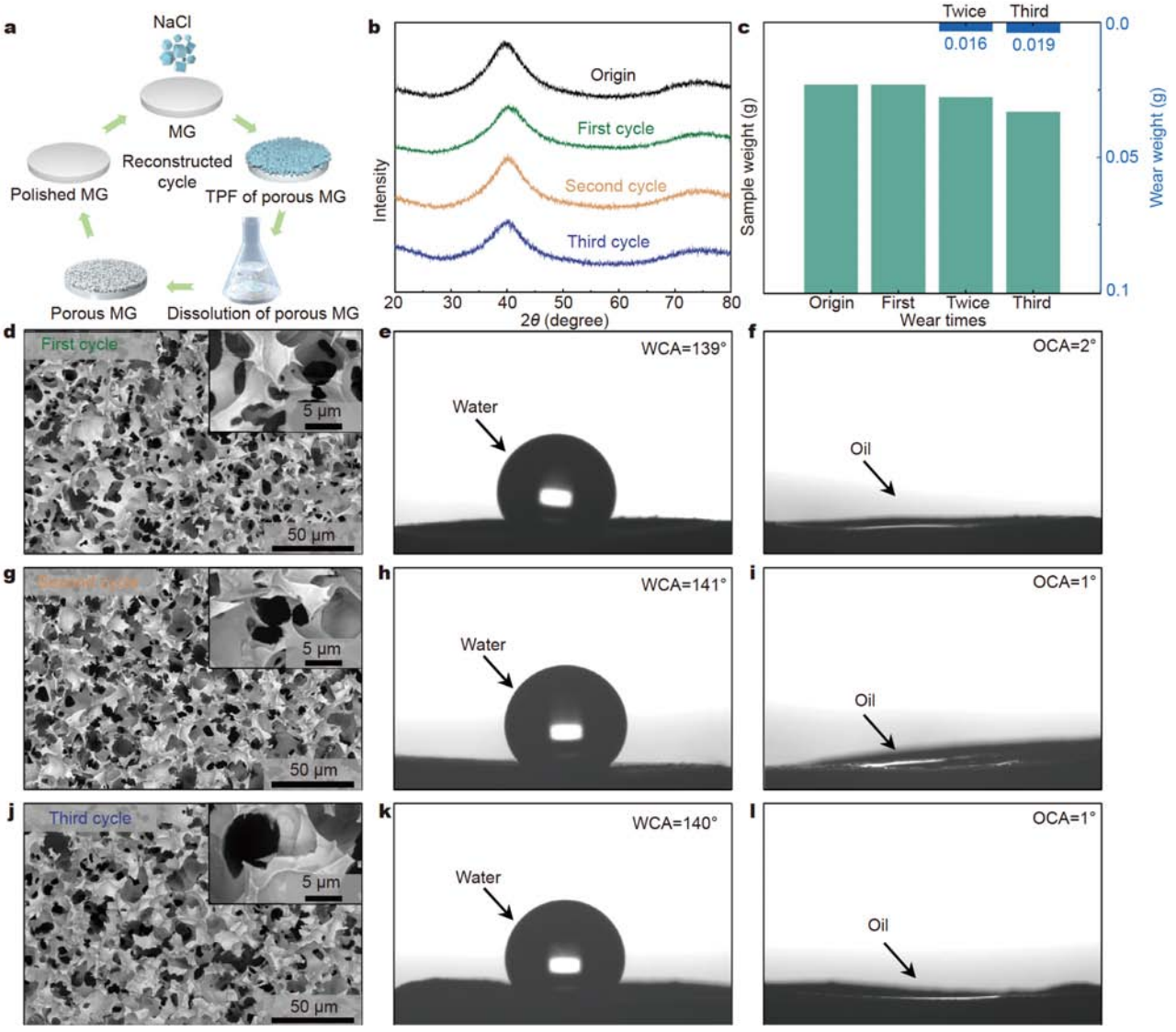

Figure 4 Reconstruction of the porous MG. (a) Schematic of porous MG reconstruction, (b) XRD pattern of the original porous MG and reconstructed porous MG, (c) weight loss of MG after surface wear. (d, g, j) Surface morphology, (e, h, k) WCA, and (f, i, l) OCA of the porous MG fabricated in the first cycle, the second cycle and the third cycle, respectively.

reconstructed for the third time using the same approach. Fig. 4j shows the SEM image of the surface morphology of the third construction, and the corresponding wettability was also tested. The WCA is ~140° and the OCA is ~0°, indicating that the reconstructed surface maintains high repeatability in performance and surface morphology. Our process demonstrates that porous MGs can be readily reconstructed even when the functional surface is destroyed, assuming that the environment has sufficient space for material use.

CONCLUSION

We successfully fabricated irregular porous structures and regular array structures on MG using a new dissolvable template strategy. The porous MG has excellent hydrophobicity and lipophilicity due to its unique porous structure and maintains excellent wettability even after being exposed to harsh environments. In addition, the porous structure can be reconstructed on the same MG due to the amorphous nature of this material. Our approach provides a new and universal route to fabricate porous structures for a wide range of applications in energy transportation and catalysis.

Received 1 June 2022; accepted 11 July 2022; published online 2 August 2022

1 Duan C, Li F, Xiao J, *et al.* Rapid room-temperature synthesis of hierarchical porous zeolitic imidazolate frameworks with high space-time yield. Sci China Mater, 2017, 60: 1205–1214
2 Pfriem N, Hintermeier PH, Eckstein S, *et al.* Role of the ionic environment in enhancing the activity of reacting molecules in zeolite pores. Science, 2021, 372: 952–957
3 Chaoui N, Trunk M, Dawson R, *et al.* Trends and challenges for microporous polymers. Chem Soc Rev, 2017, 46: 3302–3321
4 Aguila B, Sun Q, Perman JA, *et al.* Efficient mercury capture using functionalized porous organic polymer. Adv Mater, 2017, 29: 1700665
5 Duan C, Liang K, Lin J, *et al.* Application of hierarchically porous metal-organic frameworks in heterogeneous catalysis: A review. Sci China Mater, 2022, 65: 298–320

6 Zhou HC"", Kitagawa S. Metal-organic frameworks (MOFs). Chem Soc Rev, 2014, 43: 5415–5418
7 He J, Xu J, Yin J, *et al.* Recent advances in luminescent metal-organic frameworks for chemical sensors. Sci China Mater, 2019, 62: 1655–1678
8 Kasianowicz JJ, Robertson JWF, Chan ER, *et al.* Nanoscopic porous sensors. Annu Rev Anal Chem, 2008, 1: 737–766
9 Choi HK, Lee A, Park M, *et al.* Hierarchical porous film with layer-by-layer assembly of 2D copper nanosheets for ultimate electromagnetic interference shielding. ACS Nano, 2021, 15: 829–839
10 Lin Z, Liu J, Peng W, *et al.* Highly stable 3D $Ti_3C_2T_x$ MXene-based foam architectures toward high-performance terahertz radiation shielding. ACS Nano, 2020, 14: 2109–2117
11 Wang S, Xu M, Peng T, *et al.* Porous hypercrosslinked polymer-TiO_2-graphene composite photocatalysts for visible-light-driven CO_2 conversion. Nat Commun, 2019, 10: 676
12 Ma G, Yan X, Li Y, *et al.* Ordered nanoporous silica with periodic 30–60 nm pores as an effective support for gold nanoparticle catalysts with enhanced lifetime. J Am Chem Soc, 2010, 132: 9596–9597
13 Yang H, Wang C, Hu F, *et al.* Atomic-scale Pt clusters decorated on porous α-$Ni(OH)_2$ nanowires as highly efficient electrocatalyst for hydrogen evolution reaction. Sci China Mater, 2017, 60: 1121–1128
14 Zhang X, Lu W, Da J, *et al.* Porous platinum nanowire arrays for direct ethanolfuel cell applications. Chem Commun, 2009, 195–197
15 Liu L, Pippel E, Scholz R, *et al.* Nanoporous Pt-Co alloy nanowires: Fabrication, characterization, and electrocatalytic properties. Nano Lett, 2009, 9: 4352–4358
16 Burton M, Selvam A, Lawrie-Ashton J, *et al.* Three-dimensional nanostructured palladium with single diamond architecture for enhanced catalytic activity. ACS Appl Mater Interfaces, 2018, 10: 37087–37094
17 Akbar S, Elliott JM, Rittman M, *et al.* Facile production of ordered 3D platinum nanowire networks with "single diamond" bicontinuous cubic morphology. Adv Mater, 2013, 25: 1160–1164
18 Klement W, Willens RH, Duwez P. Non-crystalline structure in solidified gold-silicon alloys. Nature, 1960, 187: 869–870
19 Wang WH, Dong C, Shek CH. Bulk metallic glasses. Mater Sci Eng-R-Rep, 2004, 44: 45–89
20 Inoue A, Takeuchi A. Recent development and application products of bulk glassy alloys. Acta Mater, 2011, 59: 2243–2267
21 Ma J, Yang C, Liu X, *et al.* Fast surface dynamics enabled cold joining of metallic glasses. Sci Adv, 2019, 5: eaax7256
22 Li X, Wei D, Zhang JY, *et al.* Ultrasonic plasticity of metallic glass near room temperature. Appl Mater Today, 2020, 21: 100866
23 Zhang L, Qiu L, Zhu Q, *et al.* Insight into efficient degradation of 3,5-dichlorosalicylic acid by Fe-Si-B amorphous ribbon under neutral condition. Appl Catal B-Environ, 2021, 294: 120258
24 Fu J, Yang J, Wu K, *et al.* Metallic glue for designing composite materials with tailorable properties. Mater Horiz, 2021, 8: 1690–1699
25 Huang Z, Fu J, Li X, *et al.* Ultrasonic-assisted rapid cold welding of bulk metallic glasses. Sci China Mater, 2022, 65: 255–262
26 Li H, Li Z, Yang J, *et al.* Interface design enabled manufacture of giant metallic glasses. Sci China Mater, 2021, 64: 964–972
27 Kumar G, Tang HX, Schroers J. Nanomoulding with amorphous metals. Nature, 2009, 457: 868–872
28 Yan Y, Wang C, Huang Z, *et al.* Highly efficient and robust catalysts for the hydrogen evolution reaction by surface nano engineering of metallic glass. J Mater Chem A, 2021, 9: 5415–5424
29 Ma J, Yi J, Zhao DQ, *et al.* Large size metallic glass gratings by embossing. J Appl Phys, 2012, 112: 064505
30 Chu JP, Wijaya H, Wu CW, *et al.* Nanoimprint of gratings on a bulk metallic glass. Appl Phys Lett, 2007, 90: 034101
31 Fu G, Tor SB, Loh NH, *et al.* Fabrication of robust tooling for mass production of polymeric microfluidic devices. J Micromech Microeng, 2010, 20: 085019
32 Schroers J. Processing of bulk metallic glass. Adv Mater, 2010, 22: 1566–1597
33 Brothers AH, Dunand DC. Amorphous metal foams. Scripta Mater, 2006, 54: 513–520
34 Qiu HJ, Wang JQ, Liu P, *et al.* Hierarchical nanoporous metal/metal-oxide composite by dealloying metallic glass for high-performance energy storage. Corrosion Sci, 2015, 96: 196–202
35 Jin Y, Li R, Zuo L, *et al.* Correlation between dealloying conditions and coarsening behaviors of nanoporous silver produced by chemical dealloying of Ca-Ag metallic glass. J Alloys Compd, 2017, 695: 1600–1609
36 Meng M, Li R, Zuo L, *et al.* Fabrication of hierarchical porous metallic glasses decorated with Cu nanoparticles as integrated electrodes for high-performance non-enzymatic glucose sensing. Scripta Mater, 2021, 199: 113884
37 Luo X, Meng M, Li R, *et al.* Honeycomb-like porous metallic glasses decorated by Cu nanoparticles formed by one-pot electrochemically galvanostatic etching. Mater Des, 2020, 196: 109109
38 Schroers J, Veazey C, Johnson WL. Amorphous metallic foam. Appl Phys Lett, 2003, 82: 370–372
39 Wada T, Inoue A. Formation of porous Pd-based bulk glassy alloys by a high hydrogen pressure melting-water quenching method and their mechanical properties. Mater Trans, 2004, 45: 2761–2765
40 Brothers AH, Dunand DC. Plasticity and damage in cellular amorphous metals. Acta Mater, 2005, 53: 4427–4440
41 Brothers AH, Scheunemann R, DeFouw JD, *et al.* Processing and structure of open-celled amorphous metal foams. Scripta Mater, 2005, 52: 335–339
42 Lee MH, Sordelet DJ. Synthesis of bulk metallic glass foam by powder extrusion with a fugitive second phase. Appl Phys Lett, 2006, 89: 021921
43 Lee MH, Sordelet DJ. Nanoporous metallic glass with high surface area. Scripta Mater, 2006, 55: 947–950
44 Zhou C, Datye A, Chen Z, *et al.* Atomic imprinting in the absence of an intrinsic length scale. APL Mater, 2020, 8: 111104
45 Li R, Chen Z, Datye A, *et al.* Atomic imprinting into metallic glasses. Commun Phys, 2018, 1: 75
46 Hasan M, Schroers J, Kumar G. Functionalization of metallic glasses through hierarchical patterning. Nano Lett, 2015, 15: 963–968
47 Mukherjee S, Sekol RC, Carmo M, *et al.* Tunable hierarchical metallic-glass nanostructures. Adv Funct Mater, 2013, 23: 2708–2713
48 Liu Z, Schroers J. General nanomoulding with bulk metallic glasses. Nanotechnology, 2015, 26: 145301
49 Liu X, Shao Y, Li JF, *et al.* Large-area and uniform amorphous metallic nanowire arrays prepared by die nanoimprinting. J Alloys Compd, 2014, 605: 7–11
50 Gong P, Kou H, Wang S, *et al.* Research on thermoplastic formability and nanomoulding mechanism of lightweight Ti-based bulk metallic glasses. J Alloys Compd, 2019, 801: 267–276
51 Sarac B, Bera S, Balakin S, *et al.* Hierarchical surface patterning of Ni- and Be-free Ti- and Zr-based bulk metallic glasses by thermoplastic net-shaping. Mater Sci Eng-C, 2017, 73: 398–405
52 Wenzel RN. Resistance of solid surfaces to wetting by water. Ind Eng Chem, 1936, 28: 988–994
53 Cassie ABD, Baxter S. Wettability of porous surfaces. Trans Faraday Soc, 1944, 40: 546–551
54 Wang D, Sun Q, Hokkanen MJ, *et al.* Design of robust superhydrophobic surfaces. Nature, 2020, 582: 55–59

Acknowledgements This work was supported by the Key Basic and Applied Research Program of Guangdong Province, China (2019B030302010), the National Natural Science Foundation of China (52122105, 51871157, and 51971150), and the National Key Research and Development Program of China (2018YFA0703604). The authors also thank the assistance on microscope observation received from the Electron Microscope Center of Shenzhen University.

Author contributions Fu J and Ma J conceived the idea. Ma J, Li Z, Ruan W, Ren S, Zhang Z and Liang X supervised the work. Fu J and Liu Z carried out the experiments, and Li Z, Li X, and Sun F designed the experimental setup. Wen W performed the XRD and DSC. Huang J prepared the raw material. Fu J and Li L performed the TEM. Fu J and Ma J wrote the manuscript. All authors contributed to the discussion and analyzed the results.

Conflict of interest The authors declare that they have no conflict of interest.

Supplementary information Supporting data are available in the online version of the paper.

Jianan Fu received his BSc degree from Jiangxi Agricultural University in 2019 and Master degree in mechanical engineering from Shenzhen University in 2022. He will pursue a PhD degree at the Southern University of Science and Technology. His research includes the formation of micro/nano-structure *via* the thermoplastic forming process and the application of metallic glasses.

Jiang Ma received his BSc degree in materials science and engineering from the Southeast University in 2009 and PhD degree from the Institute of Physics, Chinese Academy of Sciences (CAS), Beijing, China, in 2014, honored with the Outstanding PhD student Award (Top 1%) and the Institute Director Award (Top 5%). He is currently a professor at the College of Mechatronics and Control Engineering, Shenzhen University, China, and received the Outstanding Teacher Award of Shenzhen, in 2018. His research includes the formation, functional application and high frequency dynamic loading behavior of metallic glasses.

溶解制造多孔金属玻璃

傅佳男[1], 李真[2], 刘泽航[1], 李信[1], 温文馨[1], 孙飞[1], 李路遥[1], 黄金标[1], 阮文清[1], 任帅[1], 张振轩[1], 梁雄[1], 马将[1*]

摘要 简单、精密、可控的制造技术在功能表面中具有广阔的应用前景. 在这项工作中, 我们通过使用食盐这种水溶性材料作为模板, 利用金属玻璃优异的热塑成型性能, 成功地实现了多孔金属玻璃的溶解制造. 通过这种溶解制造方法制备的微/纳米结构具有良好的可调控性, 不仅可以制备大面积多孔结构, 还可以制备具有纳米级复制精度的有序规则阵列. 其中, 通过可溶性模板策略制备的无序多孔结构具有约140°的水滴接触角和接近于0°的油滴接触角, 可用于油水分离, 并且在强酸和强碱的环境中浸泡后表现出稳定的润湿性. 即使在严重磨损后, 带有多孔结构的表面仍可保持约130°的水滴接触角和约4°的油滴接触角. 此外, 该策略显示出优异的可重复使用性能. 通过在同一个金属玻璃表面上重构三次多孔结构, 发现每次重构的多孔结构的润湿性没有显著变化. 本文的研究成果为制备多级孔结构及功能表面提供了一种简便可控的方法.